JOURNAL OF AIRCRAFT
Vol. 42, No. 6, November–December 2005

# Robust Aeroelastic Match-Point Solutions Using Describing Function Method

Dario H. Baldelli*
*ZONA Technology, Inc., Scottsdale, Arizona 85251*
Richard C. Lind†
*University of Florida, Gainesville, Florida 32611*
and
Martin Brenner‡
*NASA Dryden Flight Research Center, Edwards, California 93523-0273*

**A general nonlinear feedback framework to compute robust match-point solutions for aeroelastic/aeroservoelastic systems including uncertain and nonlinear operators is presented. Augmentation of the current match-point solution approach is sought using the $\mu$ method with nonlinear memoryless operators. An aeroelastic/aeroservoelastic model is built by proper interconnection of several linear fractional transformations, so that aerodynamic and structural nonlinear effects can be incorporated into a robust analysis setup. The describing function technique is used to determine the stability boundary of the nonlinear feedback system, so that limit-cycle oscillations (LCO) can be predicted and the boundary stability behavior characterized. The resulting quasilinear model allows the computation of robust stability margins that reflects both flutter and LCO instabilities. A typical section model with control surface freeplay and uncertain structural stiffness parameters is used to demonstrate the proposed aeroelastic/aeroservoelastic modeling framework. In general, good agreement was obtained with published numerical and experimental wind-tunnel test results. Comments are provided concerning possible limitations of the proposed modeling methodology.**

## Nomenclature

| | | |
|---|---|---|
| $A$ | = | aerodynamic force matrix |
| $a$ | = | aerodynamic operator |
| $C$ | = | structural damping matrix |
| $F$ | = | closed-loop system matrix |
| $f(\cdot)$ | = | general nonlinear operator |
| $K$ | = | structural stiffness matrix |
| $k$ | = | nondimensional frequency |
| $L$ | = | aircraft's wing span |
| $l$ | = | output to nonlinear operator |
| $M$ | = | structural mass matrix |
| $m$ | = | input from nonlinear operator |
| $N(X, \omega)$ | = | sinusoidal input describing function |
| $P$ | = | nominal aeroelastic/aeroservoelastic plant |
| $p$ | = | nondimensional Laplace variable, $sL/V$ |
| $Q$ | = | generalized aerodynamic matrix force |
| $s$ | = | Laplace variable |
| $u$ | = | aeroelastic model input signal |
| $\bar{u}$ | = | noisy aeroelastic model input signal |
| $V$ | = | airspeed |
| $w$ | = | input from uncertain operator |
| $X$ | = | sinusoid amplitude |
| $y$ | = | aeroelastic model output signal |
| $\bar{y}$ | = | noisy aeroelastic model output signal |
| $z$ | = | output to uncertain operator |
| $\Gamma(\cdot)$ | = | nonlinear operator matrix |
| $\Delta$ | = | uncertainty matrix |
| $\eta$ | = | generalized coordinate vector |
| $\omega$ | = | frequency of oscillation |

Received 28 June 2004; revision received 7 October 2004; accepted for publication 7 October 2004. 

*Control Engineering Specialist. Member AIAA.
†Assistant Professor, Department of Mechanical and Aerospace Engineering. Senior Member AIAA.
‡Aerospace Engineer, Aerostructures Branch. Member AIAA.

## Introduction

LIMIT-CYCLE oscillation (LCO) has been a prevalent aeroelastic/aeroservoelastic (AE/ASE) problem on several fighter aircraft.[1–4] This phenomenon usually occurs on aircraft with external stores throughout, but not limited to, the transonic flight regime.

Complicated by the aircraft/store and flight regimes, the LCO mechanisms still remain fully analytically predictable. Production flutter engineering tools are able to predict frequency and modal composition of the LCO dynamics, but fail to predict the LCO onset as well as its oscillation amplitude.

Several modeling hypotheses have been proposed as the representative model for LCO of aircraft/wings.[5] There are the aerodynamic-driven models due to various agents such as vortex dynamics,[4] transonic shock with or without flow separation,[6] the structural-based models due to nonlinear stiffness,[7] nonlinear friction damping,[1] and others.

A novel control-oriented model using the $\mu$-analysis method was developed in Ref. 8, that considers perturbations to dynamic pressure as well as to uncertain structural and aerodynamic operators. That modeling approach was further extended to allow only dependence with the airspeed, resulting in a match-point formulation.[9]

This paper augments the current match-point solution approach using the $\mu$-analysis method with nonlinear memoryless operators. The describing function technique is used to determine the stability of the nonlinear system, so that LCO can be predicted and its stability behavior characterized. The resulting quasilinear model will be used to compute robust stability margins using the $\mu$-method that reflect both flutter and LCO instabilities.

The concept involves a representation of the AE/ASE dynamics that includes both linear and nonlinear components using several linear fractional transformations (LFT). Hence, the associated nonlinear feedback model is capable of accounting for nonlinearities due to aerodynamic and structural origins.

In addition, this control-oriented setup allows optimal estimates of these nonlinear operators, identified from wind-tunnel/flight data,

that is, strain-gauge and/or accelerometer measurements, among others,[10,11] to be incorporated in an unified robust match-point solution. In that case, a data-based model updating approach is sought, that is, a technique to augment existing production flutter models of actual aircraft with nonlinear operators derived by analyzing flight-test data. That specific approach will not be further pursued in this work.[12]

To illustrate the modeling framework for flutter and LCO detection, as well as for LCO stability characterization, the proposed technique is applied to a typical section with control surface freeplay and uncertain stiffness parameters. This case study shows how uncertainty and freeplay operators can be employed to explain the mismatch between simulated and wind-tunnel test data. Good agreement was obtained with published numerical and experimental wind-tunnel test results.[13]

## Match-Point Solutions for Robust Flutter

A general framework for the analysis of nonlinear feedback models is assumed by using several LFTs. In essence, an LFT is a matrix function that is very useful for management of complex dynamic systems, and it is used as a means of standardizing a wide variety of feedback configurations.[14]

Let $P$, $\Delta$, and $\Gamma(\cdot)$ denote either nominal transfer matrices representing the system or complex matrices used to describe the associated uncertainties, or nonlinear memoryless operators, shown in Figs. 1a and 1b. The lower LFT, denoted as $F_l[P, \Gamma(\cdot)]$, is the transfer function between the signals $u$ and $y$, which is obtained by closing the lower loop through the nonlinear operator $\Gamma(\cdot)$. On the other hand, the upper LFT, $F_u(P, \Delta)$, is obtained when these signals are related by closing its upper loop through the uncertainty operator $\Delta$. In general, the lower LFT is defined as

$$F_l[P, \Gamma(l)] \triangleq P_{11} + P_{12}\Gamma(l)[I - P_{22}\Gamma(l)]^{-1}P_{21} \tag{1}$$

$$P = \begin{bmatrix} P_{11} & P_{12} \\ P_{21} & P_{22} \end{bmatrix} \tag{2}$$

whenever $\det[I - P_{22}\Gamma(l)] \neq 0$. Equivalently, an upper LFT is defined as

$$F_u(P, \Delta) \triangleq P_{22} + P_{21}\Delta(I - P_{11}\Delta)^{-1}P_{12} \tag{3}$$

whenever $\det(I - P_{11}\Delta) \neq 0$.

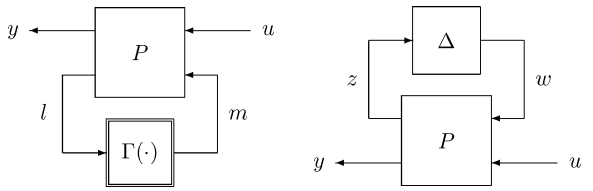


**a) Lower** **b) Upper**

**Fig. 1 Linear fractional transformation operators.**

Similarly, a given AE/ASE system can be generated by a proper interconnection of several LFTs. The associated model contains information on the structural model, the unsteady aerodynamic rational approximation, the flight-control systems, as well as the interconnection structure and exogenous signals. In Ref. 9 a model formulation is introduced that results in match-point solutions using the $\mu$-method analysis. The modeling process starts with the aeroelastic equations of motion of the nominal nonlinear system written in the Laplace domain,

$$M\ddot{\eta} + C\dot{\eta} + K\eta + f(\eta) = -\bar{q}_\infty Q(p)\eta \tag{4}$$

where $M \in \mathbb{R}^{n\times n}$, $C \in \mathbb{R}^{n\times n}$, and $K \in \mathbb{R}^{n\times n}$ are the generalized mass, damping, and stiffness structural matrices; $\boldsymbol{\eta} \in \mathbb{R}^n$ is the vector of generalized coordinates; $n$ is the number of elastic modes; and $f(\boldsymbol{\eta})$ is the nonlinear operator as a function of the generalized coordinates. In addition, $Q(p)$ is the aerodynamic force coefficient (AFC) matrix, and $\bar{q}_\infty$ is the aerodynamic pressure. The most general rational function approximation of the AFC matrix is

$$Q(p) = A_0 + A_1 p + A_2 p^2 + D(Ip - R)^{-1}Ep \tag{5}$$

where $p = sL/V$ and all of the coefficient matrices are real. Because the aerodynamic data are given for harmonic oscillations, the approximation process involves the replacement of $p$ by $ik$, where $k$ is the nondimensional frequency $\omega L/V$. Least-squares procedures are used to compute the matrix approximation coefficients $A_0$, $A_1$, $A_2$, $D$, $E$, and $R$. For example, when the Roger's formulation with two lag terms is used, the $D$, $E$, and $R$ matrices are as follows[15,16]:

$$D = [\,I \quad I\,], \qquad E = \begin{bmatrix} A_3 \\ A_4 \end{bmatrix}, \qquad R = -\begin{bmatrix} \beta_1 & 0 \\ 0 & \beta_2 \end{bmatrix} \tag{6}$$

Now, the equation of motion is broken down into several LFT subsystems to incorporate uncertain and nonlinear operators in the aeroelastic system. The devised nonlinear feedback AE/ASE system is shown in Fig. 2. The structural dynamics are represented by the linear matrix coefficients $S$, uncertainty block $\Delta_S$, as well as a nonlinear operator $\Gamma_s(\cdot)$. In the same way, the unsteady aerodynamic loads can be described by the linear element $A$; a parametric uncertainty around the airspeed perturbation parameter $\delta_V$; an uncertainty block $\Delta_A$ associated with the lag terms $\beta_i$, $i = 1, 2$; and the nonlinear operator $\Gamma_A(\cdot)$. Additionally, the flight-control system is described by $K$. This model also contains excitation and sensing uncertainties denoted $\Delta_o$ and $\Delta_i$. Of course, any prior knowledge about actuator or sensor nonlinearities should then be modeled using an actuator/sensor LFT, as proposed for the structural and nonlinear operators.

In this work, the proposed nonlinear feedback framework will allow the analysis of the linear components with uncertain and nonlinear operators. This analysis is actually simplified using the LFT framework. For example, the nominal aeroelastic model $P$

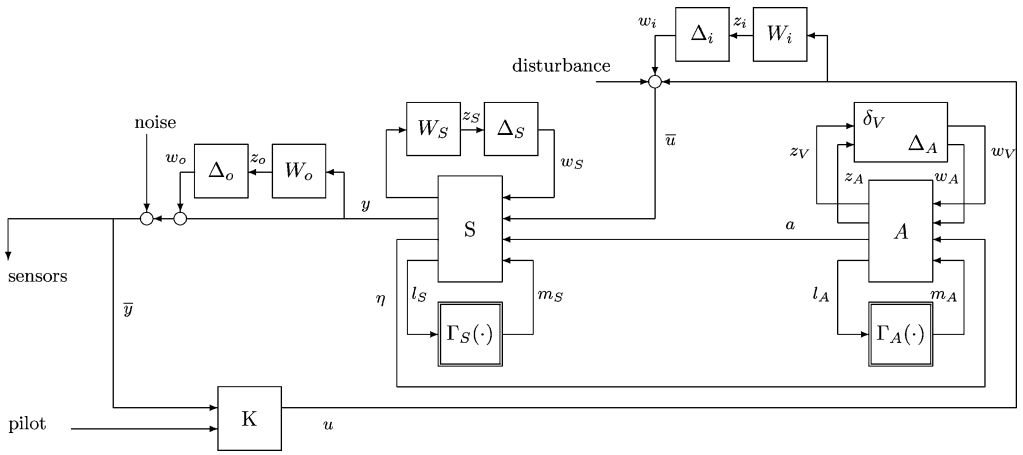


**Fig. 2 General aeroservoelastic system with uncertainties and nonlinearities.**

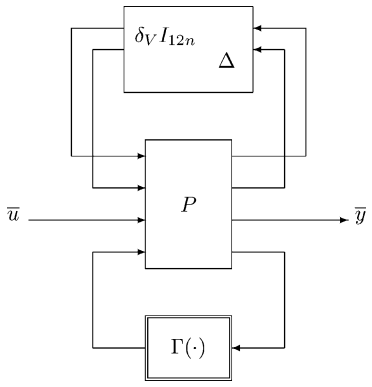


**Fig. 3 Model for $\mu$ analysis.**

is obtained by composing the operators $S$ and $A$ with the input and output weighting matrices $W_i$ and $W_o$ through LFT algebra $[\Delta_s = \Delta_A = \Delta_o = \Delta_i = \Gamma_S(\cdot) = \Gamma_A(\cdot) = K \equiv 0]$. This nominal linear model is parameterized around the airspeed perturbation parameter $\delta_V$ and can be analyzed by itself to determine a traditional flutter margin. Combining the nominal aeroelastic plant $P$ with the uncertainty matrices $\Delta_S$, $\Delta_A$, $\Delta_i$, and $\Delta_o$, enables an aeroelastic LFT model, parameterized around $\delta_V$, to compute the robust stability margin $[\Gamma_S(\cdot) = \Gamma_A(\cdot) = K \equiv 0]$. Finally, the nonlinearities can be included such that analyzing the aeroelastic LFT interconnection of $P$ with $\Delta_A$, $\Delta_S$, $\Delta_i$, $\Delta_o$, $\Gamma_A(\cdot)$, and $\Gamma_S(\cdot)$, allows stability margin computations for LCOs with uncertainties. The resulting LFT model is a function of a single parameter $\delta_V$ that describes the flight condition. Also, any of these models can be augmented for aeroservoelastic analysis by including the controller given by $K$.

Figure 3 shows the nonlinear feedback aeroelastic model ($K = 0$) related to the airspeed parameter $\delta_V$, obtained by blending all uncertainty and nonlinear operators into the block diagonal matrices $\Delta$ and $\Gamma(\cdot)$. It can be observed that there are $12n$ instances of velocity perturbation that arise from the unsteady aerodynamic operator $A$ (Ref. 9). In this case, the uncertainty matrix $\Delta$ presents the following structure:

$$\Delta = \begin{bmatrix} \Delta_S & 0 & 0 & 0 \\ 0 & \Delta_A & 0 & 0 \\ 0 & 0 & \Delta_o & 0 \\ 0 & 0 & 0 & \Delta_i \end{bmatrix} \tag{7}$$

where $\Delta_S$ and $\Delta_A$ are the structural and aerodynamic uncertainty blocks

$$\Delta_S = \begin{bmatrix} \Delta_M & 0 & 0 \\ 0 & \Delta_C & 0 \\ 0 & 0 & \Delta_K \end{bmatrix} \tag{8}$$

$$\Delta_A = \begin{bmatrix} \Delta_{\beta 1} & 0 \\ 0 & \Delta_{\beta 2} \end{bmatrix} \tag{9}$$

with $\Delta_i$, $i = M, C, K, \beta_1, \beta_2$, the modeling uncertainties related to the mass, damping, stiffness, and unsteady aerodynamic lag matrices, respectively. The nonlinear operator matrix $\Gamma(\cdot)$ is defined as

$$\Gamma(\cdot) = \begin{bmatrix} \Gamma_S(\cdot) & 0 \\ 0 & \Gamma_A(\cdot) \end{bmatrix} \tag{10}$$

Then, the nominal aeroelastic plant $P$ is defined through the relationship between the related input and output signals as

$$\begin{Bmatrix} z_t \\ \bar{y} \\ l_t \end{Bmatrix} = P \begin{Bmatrix} w_t \\ \bar{u} \\ m_t \end{Bmatrix} \tag{11}$$

where $\boldsymbol{z}_t^T = \{z_V, \boldsymbol{z}_S^T, \boldsymbol{z}_A^T, \boldsymbol{z}_o^T, \boldsymbol{z}_i^T\}^T$, $\boldsymbol{l}_t = \{\boldsymbol{l}_S^T, \boldsymbol{l}_A^T\}^T$, $\boldsymbol{w}_t^T = \{\boldsymbol{w}_V, \boldsymbol{w}_S^T \boldsymbol{w}_A^T, \boldsymbol{w}_o^T, \boldsymbol{w}_i^T\}^T$, and $\boldsymbol{m}_t = \{\boldsymbol{m}_S^T, \boldsymbol{m}_A^T\}^T$ are the associated uncertainty and nonlinear operator input and output vectors. In addition, $\bar{\boldsymbol{u}}$ and $\bar{\boldsymbol{y}}$ denote the aeroelastic model input and output vectors chosen by the designer. In this way, the proposed modeling and analysis framework allows the designer to take into account the effect of common concentrated nonlinearities in the AE/ASE systems easily, that is, freeplay and rate-limit effects on the aircraft's control surfaces.

## LCO Prediction by Nonlinear Feedback AE/ASE Model

The proposed nonlinear modeling framework is suitable for the describing function method, allowing the frequency domain techniques to be applied to detect LCO.[17,18] The method provides a linear approximation to the generic nonlinear element $\Gamma(\cdot)$ based on the assumption that the input to the nonlinear element is a known sinusoidal of constant amplitude. Then, the fundamental harmonic of the element's output is compared with the input sinusoid to determine the steady-state amplitude and phase relation. This relationship is defined as the sinusoidal input describing function (SIDF) for the nonlinear element.[19]

Assume that the input to the nonlinear element is a sinusoidal signal $x(t) = X \sin(\omega t)$, where $X$ is the amplitude of the input sinusoid and $\omega$ is its frequency. Suppose that the nonlinear element output is periodic with the same period as its input and that it may be expanded in the Fourier series

$$y(t) = A_0 + \sum_{k=1}^{\infty} Y_k \sin(k\omega t + \phi_k) \tag{12}$$

Thus, $y(t)$ consists of a fundamental component

$$Y_1 \sin(\omega t + \phi_1) \tag{13}$$

together with a mean level $A_0$ and harmonic components at frequencies $2\omega, 3\omega, \ldots, n\omega$, $n \in \mathbb{N}_+$ (positive integers). The describing function method relies on the assumption that only the fundamental harmonic is significant. This is often valid because AE/ASE systems are essentially low-pass filters. The nonlinear element is then approximately modeled by its SIDF,

$$N(X, \omega) = (Y_1/X) \angle \phi_1 \tag{14}$$

Figure 4 shows the basic system configuration used by the describing function method to detect periodic behavior, where $G(s)$ represents a generic linear transfer function of the system and $N(X, \omega)$ is the SIDF of the nonlinear operator $\Gamma(\cdot)$. Hence, the stability of the nonlinear closed-loop system can be analyzed using Nyquist's criterion applied to this quasi-linear system. The associated necessary condition of oscillation of the closed-loop system in the complex plane is obtained by solving

$$1 + N(X, \omega)G(s) = 0 \tag{15}$$

for a particular amplitude $X$ and frequency $\omega$ of the LCO. Equation (15) is denoted as the first-order harmonic balance equation.

In general, simple nonlinearities are characterized by a zero phase angle between the input and output, and by a lack of dependence on the frequency of the input sinusoid.[17] In these cases, in the $G(j\omega)$ complex plane, the locus traced out by $-1/N(X)$ as $X$ varies is being considered a generalization of the $(-1, j0)$ condition in the linear case.[20] Consequently, for LCOs probably to exist, we must have an intersection between the polar plot of $G(j\omega)$ and the $-1/N(X)$ locus. The term probably is used because the describing function method relies on the linear approximation of the nonlinear operator.

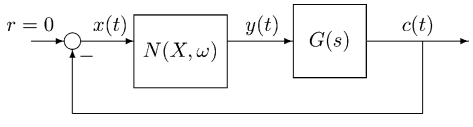


**Fig. 4 Quasilinear system for periodic behavior detection.**

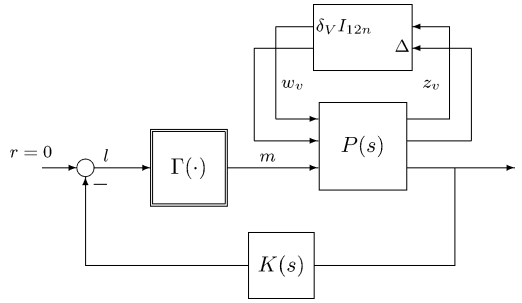


**a) Nonlinear uncertain system parameterized around airspeed**

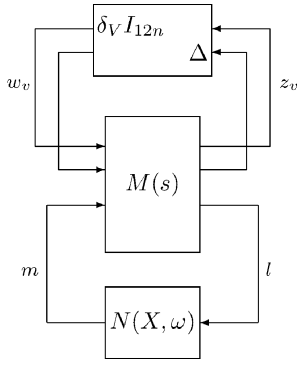


**b) Aeroservoelastic system parameterized around airspeed**

**Fig. 5 Quasilinear uncertain system for periodic behavior detection.**

Thereby, additional analysis could be needed to ensure that a certain periodic solution is achieved through the parameters $(X, \omega)$ at the input of the nonlinear operator.[19,21]

Measures of robustness for nonlinear systems with describing functions can be determined using linear tools. Consider replacing the linear aeroelastic dynamic $G(s)$ with its uncertain representation given by the nominal aeroelastic plant $P$ and associated uncertainty operator $\Delta_v = \text{diag}(\delta_V, \Delta)$, where $\Delta$ is defined in Eq. (7). Then, a generalized condition of oscillation for the proposed nonlinear AE/ASE model is obtained using the $\mu$-analysis method.[18] Figure 5a shows the general interconnection structure for the uncertain nonlinear system. In this block diagram, $F_u[P(s), \Delta_v]$ represents the uncertain aeroelastic model, $G(s)$ and $K(s)$ are the flight-control system, and $\Gamma(\cdot)$ represents a block diagonal matrix whose elements on the main diagonal are the memoryless nonlinear operators. In Fig. 5b, the block $M(s)$ is obtained by combining the linear elements $P(s)$ and $K(s)$ using suitable LFT algebra, and $N(X, \omega)$ is the related block-diagonal SIDF of the matrix of nonlinearities $\Gamma(\cdot)$. Now, under the assumption of the first harmonic approximation, the necessary condition for the existence of LCO is defined as

$$\det\{I - F_l[M(j\omega), N(X, \omega)]\Delta_v\} = 0 \tag{16}$$

This is recast in the $\mu$ framework as a robust stability condition of the lower LFT, $F_l\,[M(j\omega), N(X, \omega)]$, whereas it is subject to the allowable variation of the airspeed through the parameter $\delta_V$ in $\Delta_v$ for a fixed $\Delta$. Then it is necessary to find the minimal size perturbation $\delta_V$ that renders the determinant noted in Eq. (16) singular. This size is obtained as[18]

$$r(X, \omega) = 1/(\mu\{F_l[M(j\omega), N(X, \omega)]\}) \tag{17}$$

where $r(X, \omega)$ can also be considered a robustness margin that measured the smallest airspeed perturbation $\delta_V$ for which a necessary condition of oscillation is obtained. Then, an LCO condition is sought by fixing $X$ and $\omega$ and driving the least damped eigenvalues of the $F_l[M(j\omega), N(X, \omega)]$ to the imaginary axis by varying the perturbation parameter $\delta_V$. The LCO prediction is characterized by the airspeed, and the amplitude and frequency of oscillation are characterized through the set of parameters $(\delta_V,\ X,\ \omega)_{|\text{LCO}}$.

## LCO Stability Characterization

In this section, the LCO stability characterization is performed using the setup shown in Fig. 5b. It is conjectured that the aircraft's observed nonlinear oscillations can be classified as a subcritical Andronov–Hopf bifurcation (see Ref. 22). This bifurcation of LCO from an equilibrium point occurs when a pair of complex-conjugate eigenvalues of the linearized system crosses the imaginary axis into the right-hand side of the complex plane as the airspeed is varied.[23] Then, the stability characterization stage closely follows the framework developed by Anderson.[24] It is based on a spectral decomposition of the related state-space description of the quasilinear AE/ASE system, and the evolution of LCO will be evaluated as a function of a critical system parameter $\delta_V$. In the following paragraphs, the key is to find out how the real part of the eigenvalues of the nominal or uncertain quasilinear AE/ASE system change when the solution is perturbed.

To this end, the state-space realization between the input $m$ and the output $l$, which represents the linear part of the system, is obtained from the LFT interconnection displayed in Fig. 5b. That is,

$$\dot{x} = Ax + Bm \tag{18}$$

$$l = Cx \tag{19}$$

where $(A, B, C, 0)$ is the state-space description of the upper linear fractional transformation $F_u(M, \Delta_v)$ and $x$ is the state trajectory. In the following paragraphs, it will be assumed that the nonlinear element is only a function of the amplitude $X$ of the input signal. This assumption does not limit the applicability of the proposed LCO characterization framework because many simple and complex memoryless operators usually present in actual AE/ASE plants have SIDF that are frequency independent. Therefore, the quasi-linear part of the system is given by

$$m = N(X)l \tag{20}$$

When the linear and quasilinear parts of the AE/ASE system are combined, the equations of the closed-loop system are obtained as

$$\dot{x} = [A + BN(X)C]\,x = Fx \tag{21}$$

It turns out that the limit-cycle behavior is obtained from the derivatives of the eigenvalues of $F, \lambda_i = \sigma \pm j\omega$, located on the imaginary axis (with $\sigma = 0$ and $\omega = \omega_{\text{LCO}}$ at the LCO condition). In Ref. 24, it is shown that by computation of the spectral decomposition of the $F$ matrix,

$$F = \sum_{k=1}^{n} \lambda_k \boldsymbol{u}_k \boldsymbol{v}_k^T \tag{22}$$

where the right and left eigenvectors $\boldsymbol{u}_k$ and $\boldsymbol{v}_k^T$ are defined as

$$\lambda_k \boldsymbol{u}_k = F\boldsymbol{u}_k, \qquad \boldsymbol{v}_k^T \lambda_k = \boldsymbol{v}_k^T F \tag{23}$$

and under the assumption of orthogonal and proper normalization properties of the eigenvectors $(\boldsymbol{v}_k^T \boldsymbol{u}_k, k = 1, \ldots, n)$, the stability condition is computed from

$$\frac{\partial \sigma}{\partial \rho} = Re\left[ v_k^T B \frac{\partial N(X)}{\partial \rho} C u_k \right] \tag{24}$$

where $\rho$ is a small perturbation parameter for $F$. In Eq. (24), $\partial N(X)/\partial\rho$ is the partial derivative of the SIDF with respect to the same parameter, being, in this case, the amplitude of the output signal $l$. Hence, the stability criteria states that a stable LCO is obtained when $\partial N(X)/\partial\rho < 0$, and, conversely, an unstable limit cycle results when $\partial N(X)/\partial\rho > 0$, that is, if after being perturbed the state trajectory $x(t)$ tends toward the limit cycle as $t \to \infty$, then it is a stable LCO, otherwise it is an unstable LCO.

Note that, by fixing the SIDF's amplitude $X$ and the uncertain operator $\Delta$ while varying the perturbation parameter $\delta_V$, the proposed nonlinear analysis framework allows the designer to predict the LCO stability boundary, as well as to characterize its stability behavior.

## Case Study: Typical Section with Control Surface Freeplay

The testbed for the proposed LCO detection and characterization framework is a three-degree-of-freedom (DOF) typical section including a flap as a control surface.[13] The structural stiffness of the control surface includes a freeplay operator that creates a state of equilibrium between elastic, inertial, and aerodynamic forces of the aeroelastic system as the airspeed is increased. In Ref. 13, it is shown through wind-tunnel tests and numerical results, that high-amplitude (low-frequency) and low-amplitude (high-frequency) steady-state LCOs may be generated with this freeplay mechanism.

The experimental phase was conducted in a low-speed wind tunnel with airspeed ranging from 4.3 to 24 m/s. Conner et al.[7] present excellent agreement between their wind-tunnel measurements and numerical results. This indicates that the experimental data were of high quality and that the nominal structural data were highly accurate. Therefore, this three-DOF typical section with freeplay can be considered a standard benchmark case for validating nonlinear aeroelastic methodologies.

Figure 6a shows the nonlinear system that performs plunge $h(t)$, pitch $\alpha(t)$, and flap $\beta(t)$ motions, respectively. A freeplay with $\delta_0 = \pm 2.12$ deg is introduced into the control surface hinge point, which results in the restoring diagram shown in Fig. 6b. This static, single-valued nonlinearity may represent a loose hinge or linkage of the control system. The three-DOF typical section parameters are defined in Table 1.

The nonlinear system is defined in the robust match-point solutions setup by Eq. (4), where $\boldsymbol{\eta} = \{-h, \alpha, \beta\}^T$ is the generalized coordinate vector and $M$, $C$, and $K$, are the generalized mass, damping, and stiffness matrices, respectively. Their numerical values are

$$M = \begin{bmatrix} 3.2930 & 0.0859 & 0.0039 \\ 0.0859 & 0.0135 & 0.0008 \\ 0.039 & 0.0008 & 0.000326 \end{bmatrix}$$

$$C = \begin{bmatrix} 3.2962 & 0.03517 & -0.0000356 \\ 0.03517 & 0.03042 & 0.00202 \\ -0.0000356 & 0.00202 & 0.0007757 \end{bmatrix}$$

$$K = \begin{bmatrix} K_h & 0 & 0 \\ 0 & K_\alpha & 0 \\ 0 & 0 & K_\beta \end{bmatrix}$$

where $K_h = 2818.8$, $K_\alpha = 37.3$, and $K_\beta = 3.9$. In this case, only structural nonlinearity is considered, that is, if $\Gamma_A(\cdot) = 0$, then the nonlinear operator $f(\boldsymbol{\eta})$ in Eq. (4) is denoted $\Gamma_s(\boldsymbol{\eta})$. Now, the generic nonlinearity $\Gamma_s(\boldsymbol{\eta})$ is replaced with a feedback relationship, and a new model output is defined as

$$l = \boldsymbol{\eta}$$

and the nonlinearity in the model is then replaced with an input signal $m$

$$m = \Gamma_s(l)$$

Figure 7 shows the relationship between the nominal dynamics expressed by $S$, the structural parameter uncertainty block $\Delta_S$, and the nonlinear operator $\Gamma_s(\cdot)$. The input and output vectors of this LFT model are the aerodynamic operator $a = -\bar{q}_\infty Q(p)\boldsymbol{\eta}$, the generalized coordinate vector, as well as its first and second rates of change (Fig. 2). In this example, the parametric uncertainty block takes into account only possible errors in the standard $M$, $C$, and $K$ structural matrices and has a block-diagonal structure as defined by Eq. (8).

For the typical airfoil section case, the nonlinearity $\Gamma_s(\cdot)$ is a function of the flap DOF $\beta$. Given a periodic motion $\beta = \beta_s \sin \omega t$,

**Table 1 Three-DOF system parameters**

| Parameter | Value |
|---|---|
| *Geometric parameters* | |
| Chord | 0.254 m |
| Span | 0.52 m |
| Semi-chord | 0.127 m |
| Elastic axis, $a$ | −0.5 |
| Hinge line, $c$ | 0.5 |
| *Mass parameters* | |
| Mass of wing | 0.62868 kg |
| Mass of aileron | 0.18597 kg |
| Mass/length of wing-aileron | 0.1558 kg/m |
| Mass of support blocks | 0.47485 × 2 kg |
| *Inertial parameters* | |
| $S_\alpha$ (per span) | 0.08587 kg m |
| $S_\beta$ (per span) | 0.00395 kg m |
| $x_\alpha$ | 0.434 |
| $x_\beta$ | 0.01996 |
| $I_\alpha$ (per span) | 0.01347 kg m$^2$ |
| $I_\beta$ (per span) | 0.0003264 kg m$^2$ |
| $r_\alpha$ | 0.7321 |
| $r_\beta$ | 0.11397 |
| $\kappa$ | 0.03984 |
| *Stiffness parameters* | |
| $C_\alpha$ (per span) | 1486 1/s$^2$ |
| $C_\beta$ (per span) | 155 1/s$^2$ |
| $C_h$ (per span) | 1809 1/s$^2$ |
| *Reduced stiffness parameters* | |
| $K_\alpha$ | 37.3 |
| $K_\beta$ | 3.9 |
| $K_h$ | 2818.8 |

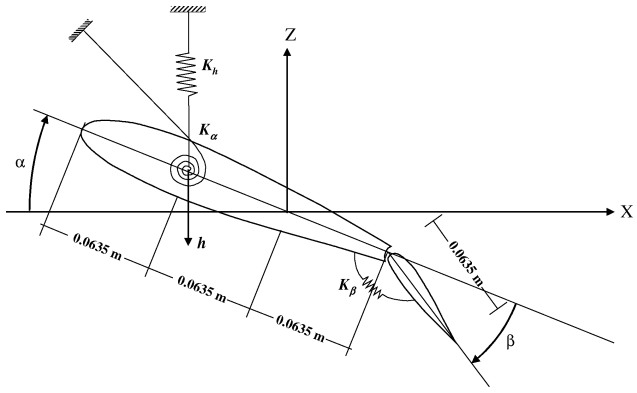


**a) Typical section, three-DOF**

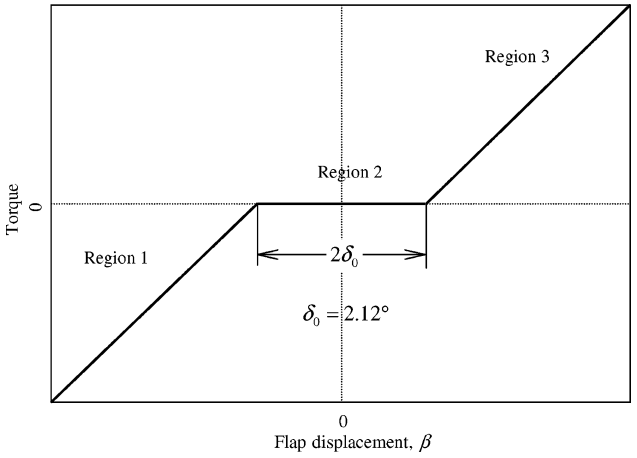


**b) Structural freeplay nonlinearity**

**Fig. 6 Pitch–plunge system with control surface freeplay.**

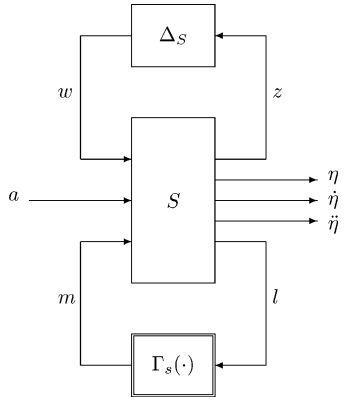


**Fig. 7 Nonlinear structural dynamic subsystem.**

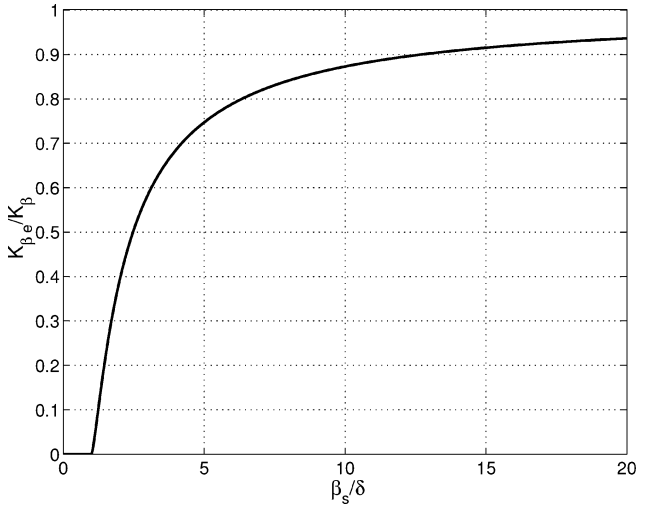


**Fig. 8 Control surface freeplay SIDF.**

the SIDF of $\Gamma_s(\beta)$ is used to model the first harmonic gain of the control surface freeplay. It is named $N(\beta_s)$, and it is shown in Fig. 8 as a function of the parameter $\beta_s/\delta$. Hence, the nominal flap stiffness $K_\beta$ is replaced by $K_{\beta_e}$ such that

$$K_{\beta_e} = N(\beta_s)\, K_\beta, \qquad K_\beta = 3.9 \tag{25}$$

$$N(\beta_s) = (1/\pi)\left[\pi - 2\sin^{-1} m - 2m\sqrt{1-m^2}\right] \tag{26}$$

where $m = \delta/\beta_s$ and $K_{\beta_e}$, $K_\beta$, and $N(\beta_s)$ are the equivalent flap stiffness, the nominal flap stiffness, and the freeplay's SIDF.[25]

*Match-Point Flutter Analysis*

The underlying two-dimensional unsteady aerodynamic is obtained using a high-aspect-ratio rectangular wing as shown in Fig. 9a using the three-dimensional frequency-domain unsteady aerodynamic method ZAERO.[16] Only the unsteady pressures along the root of the wing are selected, so that the resulting unsteady aerodynamic forces are nearly two dimensional. This is verified by comparison with the Sears function shown in Fig. 9b, where excellent agreement can be seen. ZAERO generated two-dimensional frequency-domain unsteady aerodynamics that are then transformed into a time-domain rational function form using Roger's approximation method.[15]

The eigenvalue analysis for the system when $K_\beta = 3.9N$ is shown in Fig. 10. Figure 10a shows the real part of the eigenvalues $\lambda_R$ vs airspeed $V$, whereas Fig. 10b shows the associated root locus as a function of the airspeed. It is clearly visible in Fig. 10a that the intersection of the plunge mode with the real axis occurs at the airspeed 23.19 m/s. When $V \approx 0$, the uncoupled aeroelastic mode frequencies are $\omega_h = 4.45$ Hz, $\omega_\alpha = 9.20$ Hz, and $\omega_\beta = 19.17$ Hz, respectively. In addition, the flutter frequency is observed from root-locus plot and occurs at $\omega_f = 6.019$ Hz.

**Table 2 Flutter speeds and frequencies for several linear methods**

| Flutter | Numerical: Conner et al.[7] | Numerical: Roger[15] | Test, wind tunnel[18] |
|---|---|---|---|
| Speed, m/s | 23.9 | 23.2 | 20.6 |
| Frequency, Hz | 6.11 | 6.01 | 5.47 |

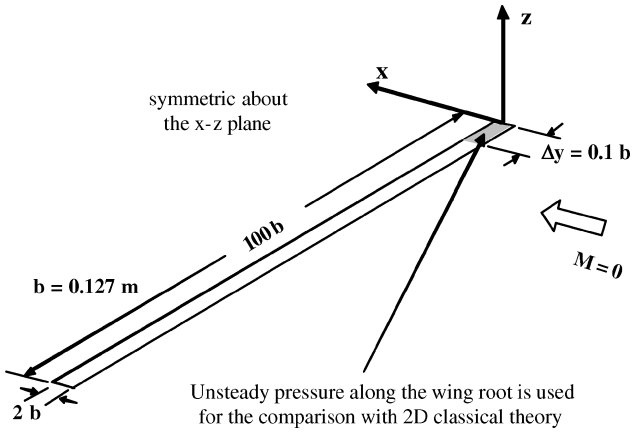


**a) High-aspect-ratio wing for two-dimensional aerodynamics**

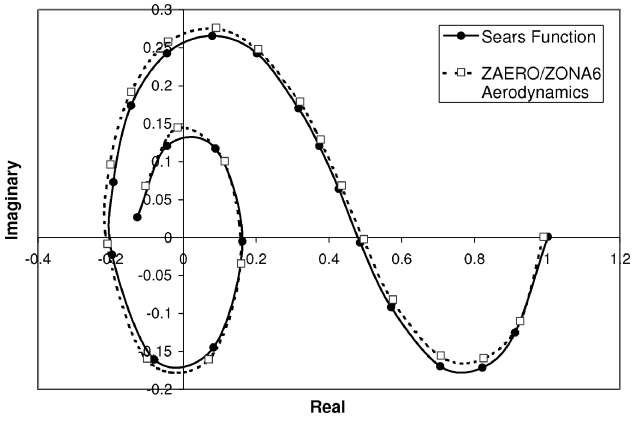


**b) Comparison of generalized aerodynamic forces between Sears function and ZONA6.**

**Fig. 9 Unsteady load generation.**

Table 2 lists a comparison of the results for the linear system ($\delta_0 = 0$) with $K_\beta = 3.9$ N using several aerodynamic force approximation methods,[7,15] as well as for the actual typical section wind-tunnel test. The differences in the predicted flutter speed based on numerical eigenvalue analysis and the measured data during the flutter wind-tunnel test are usually attributed to the freeplay nonlinearity present in the actual wing model.

Figures 11a and 11b show by the dot–dashed line the flutter speed $V_F$ and frequency $\omega_F$ vs the flap stiffness $K_\beta$ for the aeroelastic system using the match-point solution framework without freeplay and uncertainties, that is, $\Delta_S = \delta_0 \equiv 0$. They are computed using Roger's[15] formulation with two aerodynamic lag terms for each structural mode. These results are also compared with those obtained by Tang et al.[13] (dashed line). Good correlation between these sets of results are visibly noticeable, except for the abrupt change in the flutter frequency, from high to low, at $K_\beta = 1.2$ N that is slightly lower than that presented by Tang et al. ($K_\beta = 1.48$ N). This effect can be attributed to the differences in the unsteady aerodynamics computed using ZAERO and the finite state method used by Tang et al.

*Robust Match-Point Solution*

A periodic behavior condition is computed for the three-DOF typical section with freeplay, in the presence of parametric uncertainties

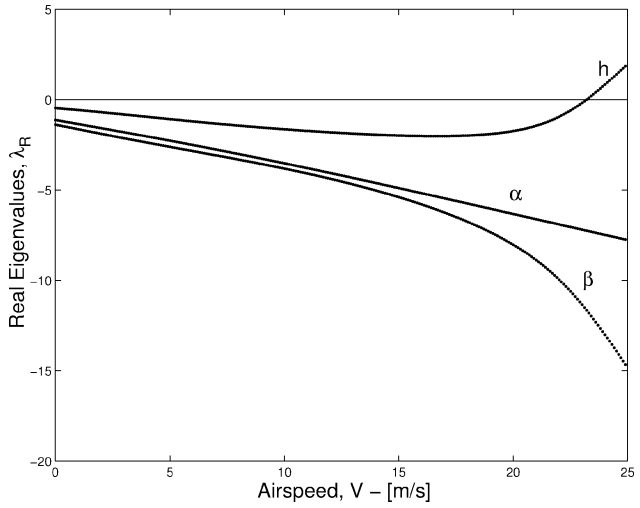


**a) Real part**

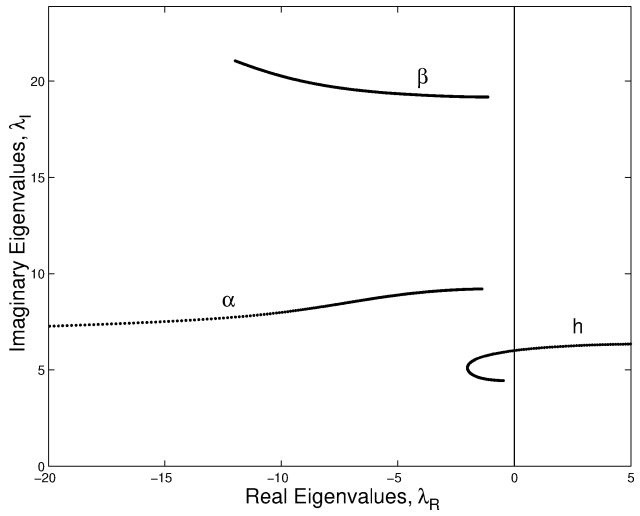


**b) Aeroelastic root locus**

**Fig. 10 Typical section with freeplay: eigenvalue solution for nominal flap stiffness ($K_\beta = 3.9$ N).**

in the structural operator. A parametric uncertainty block, $\Delta_S \neq 0$, is associated with the nominal structural matrices $M$, $C$, and $K$ of Eq. (4). The robustness margin is computed at each point $[N(\beta_s), \omega]$ of the grid, while the perturbation to airspeed $\delta_V$ is varied and the smallest destabilizing perturbation is found. The proposed analysis framework is shown in Fig. 12, and the robust stability margin is defined as[18]

$$r[N(\beta_s), \omega] = 1/\mu_{\Delta_v}\{F_l[P(j\omega), N(\beta_s)]\} \tag{27}$$

where $P$ is the linear operator resulting from the interconnection of the subsystems $S$ and $A$ shown in Fig. 2. $\Delta_v$ is given as

$$\Delta_v = \begin{bmatrix} \delta_V I_{12n} & 0 \\ 0 & \Delta_S \end{bmatrix}$$

where $\Delta_S$ is defined by Eq. (8). Figures 11a and 11b show by the solid line the evolution of the robust flutter speed $V_f$ and robust flutter frequency $\omega_f$ vs the flap stiffness $K_\beta$ for the aeroelastic system using the robust match-point solution when the freeplay's SIDF and structural stiffness uncertainty are simultaneously included. In this case study, only a 4% error in the plunge and pitch stiffness values of the typical airfoil section is considered, that is, $\Delta_K = \text{diag}(0.04, 0.04, 0)$.

Specifically, Fig. 11a shows that the computed robust flutter speeds are considerably lower than the nominal flutter values (dot–dashed line). Figure 11b shows two abrupt frequency jumps at the

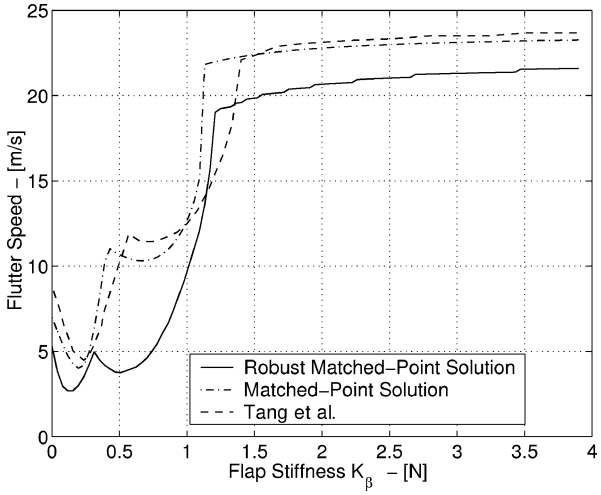


**a) Flutter speed vs $K_\beta$**

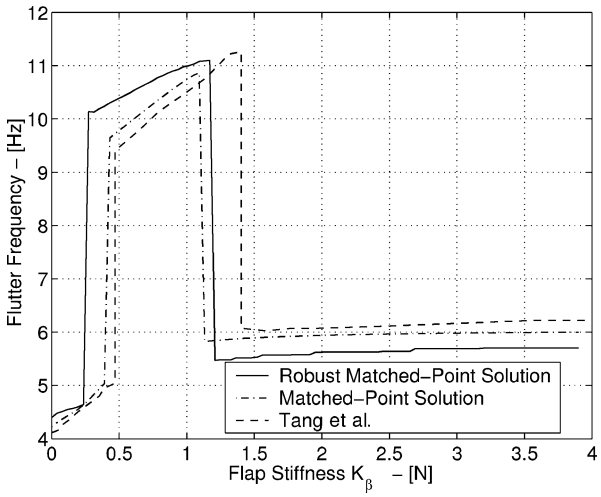


**b) Flutter frequency vs $K_\beta$**

**Fig. 11 Typical section with freeplay.**

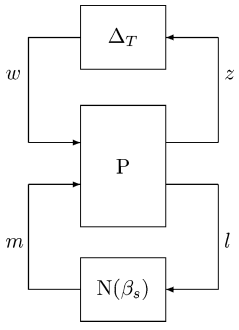


**Fig. 12 Nonlinear aeroelastic model.**

$K_\beta = 0.23$ N, from low to high flutter frequency, and at 1.21 N, from high to low flutter frequency, conditions. Consequently, these results indicate that the aeroelastic system is highly sensitive to the uncertainties in the plunge and pitch stiffness values defined by $\Delta_S$. The robust flutter indicators are lesser than the nominal flutter counterparts and demonstrate the effects of including the uncertain stiffness values in the analysis.

The computed robust flutter speed and flutter frequency parameters for the nominal flap stiffness value, $K_\beta = 3.9$ N, are shown in Table 3, and it is observed that these values are much closer to the actual results obtained in the wind-tunnel test. (See Table 2.)

Figure 13 shows the robust stability margin, $r[N(\beta_s), \omega] = 0$, when it is shown as a function of the flap stiffness and frequency parameters grid $(K_\beta, \omega)$. In this three-dimensional plot, the LCO

**Table 3 Linear and robust matched-point results**

| Flutter | Match point | | Test, wind tunnel |
|---|---|---|---|
| | Linear | Robust | |
| Speed, m/s | 23.26 | 21.6 | 20.6 |
| Frequency, Hz | 5.99 | 5.70 | 5.47 |

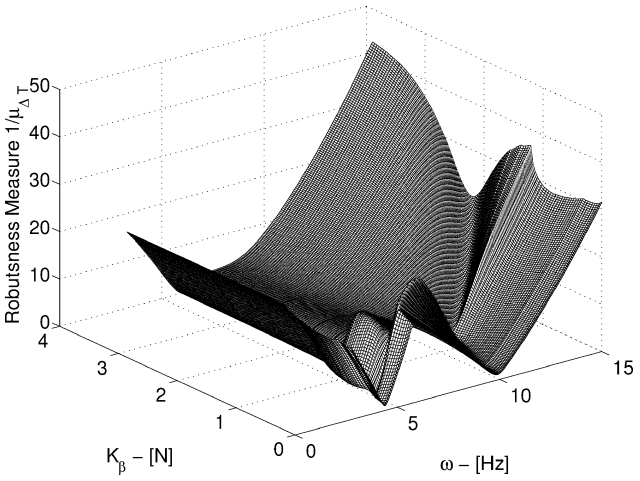


**Fig. 13 Typical airfoil section: robustness margin $r(n_\beta, \omega)$.**

condition is directly related to the robust stability margin's valleys running through the $(K_\beta, \omega)$ plane, that is, when the condition $r[N(\beta_s), \omega] = 0$ is achieved.

This case study shows how uncertainty and ideal freeplay operators can be employed to explain the mismatch between simulated and the wind-tunnel test data. Nevertheless, note that if the actual nonlinear mechanism is known, that is, by means of a nonlinear identification stage,[11] it can be replaced by its related SIDF. Then, by inclusion of this identified SIDF into the proposed robust match-point framework, it is conjectured that the resulting LCO parameters will more closely match the actual wind-tunnel test values.

#### LCO Behavior

In the two preceding sections, the existence of LCO was sought by driving the least-damped eigenvalues to the imaginary axis by varying the flight speed. In this section, the stability characterization of the LCO will be evaluated as a function of the perturbation parameter $\delta_V$ while the stability parameter $\partial\sigma/\partial\rho$ defined in Eq. (24) is used. In particular, this equation points out that the LCO stability of the uncertain quasi-linear aeroelastic system is a function of the parameter $\partial N(X)/\partial\rho$, that is, the partial derivative of freeplay's SIDF with respect to the amplitude of the signal. In this case study, its value can be computed analytically from Eq. (26) as

$$\frac{\partial N(\beta_s)}{\partial \beta_s} = \frac{4\,\delta}{\pi \beta_s^2}\sqrt{1 - \left(\frac{\delta}{\beta_s}\right)^2} \tag{28}$$

and the stability criteria requires that a stable LCO be obtained when $\partial\sigma/\partial\beta_s < 0$ and, conversely, that an unstable LCO results when $\partial\sigma/\partial\beta_s > 0$. By definition, a limit cycle is stable if the amplitude and frequency of the limit cycle tend to return to their original values after a temporary disturbance. On the other hand, the LCO is unstable for either increasing or decreasing amplitude depending on the direction of the disturbance.[17]

Therefore, the values of the nominal and robust flutter speed $V_f$ and flutter frequency $\omega_f$ computed earlier, together with the nondimensional ratio $K_{\beta_e}/K_\beta$, are used to predict the nondimensional flap LCO amplitude $\beta/\delta$ for both the nominal match-point and the robust match-point solutions.

Figure 14a shows four different regions of LCO behavior, where the unstable parts are depicted with dots and the stable regions are indicated with solid lines. Note that there are two unstable LCO branches. The first of these is between $V/V_{f0} = 0.61$ and 1, with an oscillation frequency near the plunge natural frequency, and the second unstable branch is between $V/V_{f0} = 1.64$ and 1.77, having an oscillation frequency near the pitch natural frequency. These results, obtained by applying the match-point formulation together with the stability criteria, qualitatively agree well with the Tang et al. numerical results.[13] Still, numerical differences are presumably due to differences in the computed unsteady aerodynamic approximations.

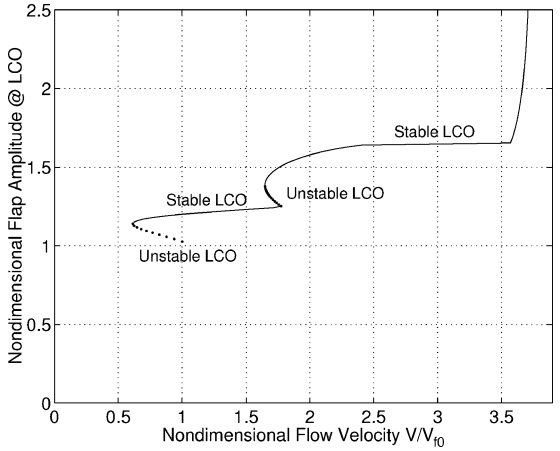


**a) Match-point solution**

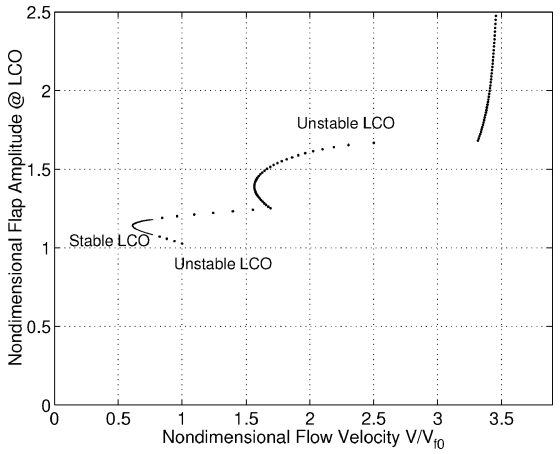


**b) Robust match-point solution**

**Fig. 14 Typical airfoil section: nondimensional flap LCO amplitude.**

In contrast, Fig. 14b shows the LCO stability behavior of the uncertain quasi-linear aeroelastic system predicted using the robust match-point solution. Contrary to the results depicted in Fig. 14a, the system is composed of mainly two unstable branches, with a small stable LCO branch between them. The first unstable LCO branch ranges between $V/V_{f0} = 0.82$ and 1, whereas the second branch spans between $V/V_{f0} = 0.84$ and 3.45. However, these results do not follow the general trend described in the conclusions of Ref. 7, that a slight change in some of the system parameters could lead to other nonlinear phenomena such as coexisting stable limit cycles. This erratic behavior of the stability parameter, $\partial\sigma/\partial\beta_s$, can be attributed to the describing function approach being based on the quasi-linear approximation of the actual nonlinear system, such that the stability behavior prediction could turn out to be conservative. Therefore, to assess the actual LCO stability behavior, additional nonlinear time simulations need to be performed.

## Conclusions

In this paper, we introduced a general nonlinear feedback framework, composed of several LFTs, to compute robust match-point solutions for AE/ASE systems including uncertain and nonlinear operators. Specifically, the approach sought to augment match-point

solutions based on the $\mu$ method with nonlinear operators. Through the proposed general LFT model, the designing engineer can easily incorporate the effect of concentrated aerodynamic and structural nonlinearities in the AE/ASE system. Then, by replacement of the nonlinear operator with its SIDF, the resulting quasilinear model is used to compute robust stability margins associated with linear and nonlinear systems. The resulting model allows the computation of stability margins that reflect both flutter and LCO instabilities. We illustrated this modeling technique with the typical section using a control surface freeplay model. The results obtained show the ability to treat a unified match-point formulation LCO prediction and its stability characterization.

## Acknowledgments

Research supported by NASA Dryden Flight Research Center under Small Business Technology Transfer Program Phase I, NAS4-03014. The authors thank the anonymous reviewers for their invaluable comments on the draft of this paper. Their suggestions considerably improved the final version.

## References

[1]Chen, P. C., Sarhaddi, D., and Liu, D. D., "Limit Cycle Oscillation Studies of a Fighter with External Stores," AIAA Paper 98-1727, 1998.

[2]Denegri, C. M., "Limit Cycle Oscillation Flight Test Results of a Fighter with External Stores," *Journal of Aircraft*, Vol. 37, No. 5, 2000, pp. 761–769.

[3]Norton, W. J., "Limit Cycle Oscillation and Flight Flutter Testing," *Proceedings of the Society of Flight Test Engineers 21st Annual Symposium*, Lancaster, CA, 1990, pp. 3.4-1–3.4-12.

[4]Cunningham, A. M., Jr., and Meijer, J. J., "Semi-Empirical Unsteady Aerodynamics for Modeling Aircraft Limit Cycle Oscillations and Other Nonlinear Aeroelastic Problems," *International Forum on Aeroelasticity and Structural Dynamics*, Vol. 2, Royal Aeronautical Society, London, June 1995, pp. 74.1–74.14.

[5]Dowell, E. H., Edwards, J., and Strganac, T. W., "Nonlinear Aeroelasticity," *Journal of Aircraft*, Vol. 40, No. 5, 2003, pp. 857–874.

[6]Edwards, J. W., Schuster, D. M., Spain, C. V., Keller, D. F., and Moses, R. W., "MAVRIC Flutter Model Transonic Limit Cycle Oscillation Test," AIAA Paper 2001-1291, 2001.

[7]Conner, D., Tang, D. M., Dowell, E. H., and Virgil, L. N., "Nonlinear Behavior of a Typical Airfoil Section with Control Surface Freeplay: A Numerical and Experimental Study," *Journal of Fluids and Structures*, Vol. 11, No. 1, 1997, pp. 89–109.

[8]Lind, R., and Brenner, M., "Robust Aeroservoelastic Stability Analysis: Flight-Test Applications," *Advances in Industrial Control*, Springer-Verlag, London, 1999, Chaps. 8, 9.

[9]Lind, R., "Match-Point Solutions for Robust Flutter Analysis," *Journal of Aircraft*, Vol. 39, No. 1, 2002, pp. 91–99.

[10]Brenner, M., and Prazenica, R. J., "Aeroservoelastic Model Validation and Test Data Analysis of the F-/A-18 Active Aeroelastic Wing," *International Forum on Aeroelasticity and Structural Dynamics*, Paper IFASD-US-32, June 2003.

[11]Baldelli, D. H., Lind, R., and Brenner, M., "Nonlinear Aeroelastic Modeling By Block-Oriented Identification," AIAA Paper 2004-1938, April 2004.

[12]Baldelli, D. H., Lind, R., and Brenner, M., "Nonlinear Aeroelastic/Aeroservoelastic Modeling by Block-Oriented Identification," *Journal of Guidance, Control, and Dynamics* (to be published).

[13]Tang, D. M., Dowell, E. H., and Virgil, L. N., "Limit Cycle Behavior of an Airfoil with a Control Surface," *Journal of Fluids and Structures*, Vol. 12, No. 7, 1998, pp. 839–858.

[14]Zhou, K., Doyle, J. C., and Glover, K., *Robust and Optimal Control*, Prentice–Hall, Upper Saddle River, NJ, 1996, Chap. 10.

[15]Roger, K. L., "Airplane Math Modeling and Active Aeroelastic Control Design," AGRAD CP-228, 1977, pp. 4.1–4.11.

[16]"ZAERO User's Manual," Ver. 7.1, ZONA Technology, Inc., Scottsdale, AZ, Aug. 2004.

[17]Graham, D., and McRuer, D., *Analysis of Nonlinear Control Systems*, Wiley, New York, 1961, Chaps. 1–5.

[18]Ferreres, G., and Fromion, V., "Nonlinear Analysis in the Presence of Parametric Uncertainties," *International Journal of Control*, Vol. 69, No. 5, 1998, pp. 695–716.

[19]Khalil, H. S., *Nonlinear Systems*, 2nd ed., Prentice–Hall, Upper Saddle River, NJ, 1996, Chaps. 1, 10.

[20]Żak, S. H., "Introduction to Analysis of Nonlinear Systems," EE-675, Lecture Notes, School of Electrical and Computer Engineering, Purdue Univ., West Lafayette, IN, Fall 2001.

[21]Mess, A. I., "Describing Functions Revisited," *IEEE Transactions on Automatic Control*, Vol. AC-20, No. 4, 1975, pp. 473–478.

[22]Wang, H. O., Abed, E. H., and Tesi, A., "Control of Bifurcations and Chaos," *The Control Handbook*, CRC Press, Boca Raton, FL, 1995, pp. 951–966.

[23]Mess, A. I., "A Plain Man's Guide to Bifurcations," *IEEE Transactions on Circuits and Systems*, Vol. CAS-30, No. 8, 1983, pp. 512–517.

[24]Anderson, M. R., "Pilot-Induced Oscillations Involving Multiple Nonlinearities," *Journal of Guidance, Control, and Dynamics*, Vol. 21, No. 5, 1998, pp. 786–791.

[25]Vidyasagar, M., "Nonlinear Systems Analysis," *Classics in Applied Mathematics*, 2nd ed., Society of Industrial and Applied Mathematics, Philadelphia, 2002, pp. 88–127.

[26]Edwards, J. W., "Transonic Shock Oscillations and Wing Flutter Calculated with an Interactive Boundary Layer Coupling Method," Euromech-Colloquium 349 Simulation of Fluid–Structure Interaction in Aeronautics, Göttingen, Germany, Sept. 1996.